Luminescence properties of Cu^{2+}-doped TMA_2MnBr_4 crystals and a spectroscopic study of the $CuBr_4^{2-}$ complexes formed

1993 J. Phys.: Condens. Matter 5 2625

(http://iopscience.iop.org/0953-8984/5/16/019)

J. Phys.: Condens. Matter 5 (1993) 2625–2642. Printed in the UK

Luminescence properties of Cu^{2+}-doped TMA_2MnBr_4 crystals and a spectroscopic study of the $CuBr_4^{2-}$ complexes formed

M C Marco de Lucas and F Rodríguez

DCITTYM (Sección Ciencia de Materiales), Facultad de Ciencias, Universidad de Cantabria, 39005-Santander, Spain

Received 9 November 1992

Abstract. This work investigates the influence of Cu^{2+} impurities on the luminescence properties of $TMA_2MnBr_4:Cu^{2+}$ as well as the local structure and orientation of the $CuBr_4^{2-}$ complexes formed, by means of the excitation and luminescence spectra, lifetime measurements and polarized optical absorption spectroscopy in the 10–300 K temperature range. It is demonstrated that the presence of an intense $Br^- \rightarrow Cu^{2+}$ charge transfer (CT) band at 555 nm strongly favours a direct energy transfer from Mn^{2+} to the non-luminescent Cu^{2+} impurities. The influence of this energy transfer on the Mn^{2+} luminescence intensity, lifetime and bandshape is analysed as a function of the Cu^{2+} concentration. The results are compared with previous ones obtained in one-dimensional Cu^{2+}-doped $TMAMnCl_3$ and $TMAMnBr_3$ crystals. Two x, y-polarized bands at 18 000 and 28 400 cm^{-1}, and two z-polarized bands at 23 800 and 36 100 cm^{-1} are observed in the CT spectra of $TMA_2MnBr_4:Cu^{2+}$. Their transition energies as well as their polarization are explained in terms of D_{2d} symmetry distortions of the $CuBr_4^{2-}$ tetrahedra. We also analyse the triplet structure observed in the first CT band which is associated with the tetrahedral $^2T_1$ CT state, which is split by the effect of both the static D_{2d} distortion and the large spin–orbit coupling of the Br^- ligands. The absence of discontinuities in the evolution of the $CuBr_4^{2-}$ CT bands with temperature supports the finding that no structural phase transition occurs below 270 K in these crystals.

1. Introduction

The synthesis of single crystals from solutions containing $(CH_3)_4NX$ and MnX_2 (X = Cl or Br) gives rise to either red $TMAMnX_3$ or green TMA_2MnX_4 crystals, depending on the crystal growing conditions and whether the stoichiometry is 1:1 or 2:1. The trihalide crystals are of great interest because they are usually employed as prototypes of one-dimensional systems. Their crystalline structure belongs to the $P6_3/m$ space group with face sharing MnX_6 octahedra forming linear chains along the hexagonal c axis. On the other hand, the TMA_2MnX_4 tetrahalides are orthorhombic ($Pmcn$ space group) at 300 K and the Mn^{2+} ions are tetrahedrally coordinated with four independent units occupying sites (4c) in the unit cell.

This different coordination around Mn^{2+} is responsible for the very intense red and green luminescence exhibited by these crystals under optical excitation into the MnX_6 or MnX_4 crystal field (CF) bands. The increase of about 3000 cm^{-1} in the Mn^{2+} ligand field strength, $10Dq$, on passing from tetrahedral to octahedral symmetry is responsible for the red shift experienced by the Mn^{2+} luminescence spectrum in these systems. However, the local structure around the Mn^{2+} is not the main influence on emission dynamics; even more important is the interaction among Mn^{2+} complexes within each structure, which

0953-8984/93/162625+18$07.50

plays a fundamental role in energy transfer. These processes have been studied in detail in the one-dimensional $TMAMnCl_3$ [1–3] and $TMAMnBr_3$ [4] crystals. These studies revealed the existence of an excitation energy transfer between the exchange coupled MnX_6 units along the chain in both crystals. The introduction of non-luminescent Cu^{2+} impurities at Mn^{2+} sites as excitation killers drastically alters their luminescence properties. A sharp decrease in the luminescence intensity as well as a progressive deviation from the single exponential behaviour of the decay is observed in these doped crystals. The higher the Cu^{2+} concentration is, the lower the luminescence intensity. An opposite effect is observed when doping with Cd^{2+}. In this situation the Cd^{2+} ions act as barriers to energy transfer, confining the migration to limited segments of the chain [2].

These phenomena, however, had not yet been investigated in TMA_2MnX_4. The reason for this probably lies in the intrinsic nature of the green Mn^{2+} luminescence expected for these crystals with *isolated* MnX_4 units. The optical properties of Cu^{2+} doped TMA_2MnCl_4 crystals have recently been reported [5] but that work was mainly focused on the dichroic nature of the optical absorption (OA) spectra of these crystals due to the presence of $CuCl_4^{2-}$ centres with D_{2d} local symmetry. Both the charge transfer (CT) spectra as well as the sensitivity of these complexes as probes for detecting the phase transition sequence undergone by this crystal in the 10–300 K temperature range were thoroughly investigated [5, 6]. A change in the crystal colour from bright green to pale orange was observed with increasing Cu^{2+} concentration due to the tail of the first CT band which peaks at 412 nm. Neither the luminescence intensity nor the lifetime of the $MnCl_4^{2-}$ was affected by the presence of Cu^{2+} impurities. However, the situation for TMA_2MnBr_4 crystals could be quite different. In fact, since the first ligand Br^- to metal Cu^{2+} CT band is expected to appear at lower energies than the one from Cl^- to Cu^{2+}; both the Cu^{2+} CT and the Mn^{2+} luminescent transitions may be resonant. Consequently, the existence of an effective energy transfer in these crystals must not be ruled out.

The aim of this work is twofold: first, to investigate the influence of Cu^{2+} impurities on the luminescence properties of TMA_2MnBr_4 crystals; and second, to characterize the Cu^{2+} complexes formed in these crystals. We focus on determining the local structure and orientation of the Cu^{2+} complexes within the lattice. For this purpose, both the CT and CF spectra associated with the formed $CuBr_4^{2-}$ complexes are analysed thoroughly by means of polarized OA spectroscopy.

An interesting aspect connected with these copper doped crystals is the ability of the CuX_4^{2-} in some crystals to present piezo- and thermochroism [7–10]. Geometrical modifications or reorientations of these distorted complexes induced by pressure or phase transitions can lead to substantial changes in the optical properties of such crystals. Furthermore, studies of the optical spectra of crystals containing tetrabromocuprates (II) are very scarce whereas a great number of compounds with $CuCl_4^{2-}$ geometries ranging from nearly tetrahedral to the square planar have been investigated [11–15].

A salient feature of the present investigations is the strong influence of the Cu^{2+} concentration on the luminescence of $TMA_2MnBr_4{:}Cu^{2+}$. Unlike $TMA_2MnCl_4{:}Cu^{2+}$, the emission spectrum of TMA_2MnBr_4 largely overlaps with the first CT band of the $CuBr_4^{2-}$ complexes. The origin of the so called *mystery bands* observed at 555 and 345 nm in the OA spectrum of nominally pure TMA_2MnBr_4 crystals [16] is clarified as being due to the presence of *uncontrolled* Cu^{2+} impurities. In fact, it is demonstrated that these mystery bands are not associated with either Mn^{2+} or possible Co^{2+} impurities, as previously suggested, but indeed correspond to CT transitions of the $CuBr_4^{2-}$ formed in $TMA_2MnBr_4{:}Cu^{2+}$.

2. Experimental details

Single crystals of pure and $CuBr_2$ doped TMA_2MnBr_4 were grown by slow evaporation at 30 °C from HBr acidic aqueous solutions containing stoichiometric amounts of $N(CH_3)_4Br$ and $MnBr_2 \cdot H_2O$. Pure TMA_2MnBr_4 crystals of bright green colour were obtained. The colour in the Cu^{2+} doped crystals varied from dark green to garnet and black with increasing Cu^{2+} concentration. The real Cu^{2+} content was measured by atomic absorption spectroscopy in three selected crystals, hereafter denoted by C1, C2 and C3. Their Cu^{2+} concentrations were 700, 2000 and 7400 ppm, respectively.

The orthorhombic crystallographic structure of all the investigated samples was checked by x-ray powder diffractograms. Several *c* and *a* plates with sizes of about $4 \times 2 \times 0.5$ mm^3 were selected and polished for optical studies. Crystal plates were characterized and oriented by means of their conoscopic images and looking for the extinction directions with a polarizing microscope.

Luminescence and excitation spectra as well as lifetime measurements were performed on an implemented Jobin Yvon JY-3D fluorimeter [17]. Decay curves were obtained by modulating the excitation light with a mechanical copper, and the luminescence signal was digitized with a Tektronix 2340A scope.

A Lambda 9 Perkin Elmer spectrophotometer equipped with Glan Taylor polarizing prisms was employed for recording the polarized optical absorption spectra. The temperature was stabilized to within 0.05 K in the 10–300 K range with a Scientific Instruments 202 closed circuit cryostat and an APD-K controller.

3. Results

The luminescence spectra at 300 K of pure and Cu^{2+} doped TMA_2MnBr_4 crystals are depicted in figure 1. The spectra consist of one asymmetric broad band whose maximum, located at about 510 nm, and intensity depend on both the Cu^{2+} concentration and the sample excitation geometry. The larger the Cu^{2+} concentration is, the shorter the maximum wavelength and luminescence intensity. The asymmetry of the band also increases with the Cu^{2+} content. The band maximum is located at 515, 512, 512 and 510 nm for the pure crystal, C1, C2 and C3, respectively. Special care was taken to record all these spectra with the same excitation geometry. All the luminescence spectra as well as the corresponding excitation spectra are nearly isotropic; the excitation peaks coincide with those observed in the OA spectrum of the pure TMA_2MnBr_4 crystal (inset of figure 1). Band labelling of the tetrahedral $MnBr_4^{2-}$ CF peaks was done according to the assignment given elsewhere [16, 18]. It is noteworthy that this OA spectrum does not show any of the so-called *mystery bands* at 345 and 555 nm previously reported [16]. However, these bands are observed in the OA spectra of the doped crystals as is shown in figure 2. The absorption coefficient of these mystery bands increases linearly with the Cu^{2+} concentration.

Like the intensity and bandshape, the luminescence decay is also very sensitive to the Cu^{2+} concentration. Figure 3 depicts the decays measured with excitation at 380 nm for the pure, C1 and C2 crystals at room temperature. The decay behaves like a single exponential for the pure and C1 crystals with associated lifetimes of 385 and 300 μs, respectively. The intensity decay for C2 is faster and clearly deviates from the single exponential behaviour. In sample C3, the luminescence intensity was so weak that we were not able to detect proper decays.

Figure 4 depicts the variation of the luminescence spectrum of the $TMA_2MnBr_4:Cu^{2+}$ (C1) crystal with temperature. Note that below about 150 K, a new emission band is

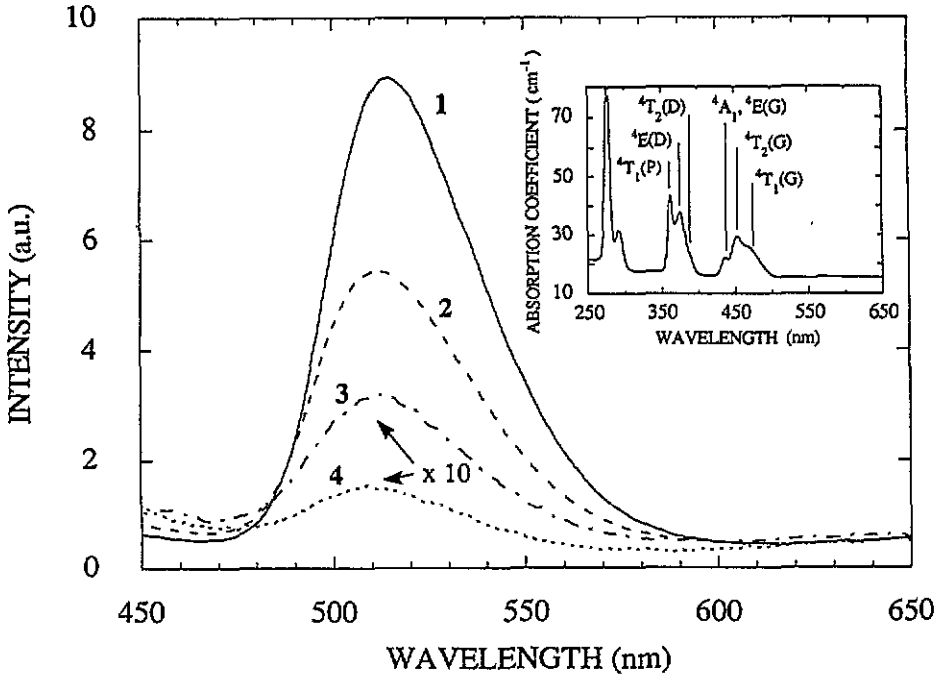

Figure 1. Room temperature luminescence spectra of the pure and Cu^{2+} doped TMA_2MnBr_4 crystals exciting at 380 nm. Spectra 1, 2, 3 and 4 correspond to the pure (0 ppm), C1 (700 ppm), C2 (2000 ppm) and C3 (7400 ppm) crystals, respectively. Spectra were recorded under the same excitation geometry. The inset shows the OA spectra of the pure crystal. Crystal field bands are labelled in T_d notation.

observed at 530 nm. Its relative intensity increases with respect to the emission band at 510 nm and dominates the spectrum at $T = 25$ K. An isosbestic point at 525 nm is present throughout the spectral evolution. It should be pointed out that though the band maximum at 25 K is located at the same position as in the pure crystal [18–20], its bandwidth at half maximum, $\Delta H = 700\ cm^{-1}$, is 300 cm^{-1} narrower.

The temperature dependence of the lifetime for both bands in the 10–300 K range is depicted in figure 5. Identical decays were measured for both emission components and neither the time dependence nor the lifetime change within our experimental accuracy throughout the temperature range.

Figure 6 shows the polarized OA spectra at 300 K in the 230–700 nm range of the Cu^{2+} doped TMA_2MnBr_4 single crystals with incident light polarized along the ***a***, ***b*** and ***c*** orthorhombic directions. In addition to the Mn^{2+} CF bands, three prominent anisotropic broad bands, hereafter called A, B and C, are observed at 555, 352 and 277 nm, respectively. Except for band A, it is more difficult to analyse the contribution of Cu^{2+} to the TMA_2MnBr_4:Cu^{2+} OA spectrum than it was in the case of the isomorphic TMA_2MnCl_4:Cu^{2+}. This is due to the stronger signal of the $MnBr_4^{2-}$ whose CF transition oscillator strengths are one order of magnitude greater than those of $MnCl_4^{2-}$ [21]. In order to solve this problem and get a more precise insight into the contribution of Cu^{2+} to the OA spectra, we have subtracted the Mn^{2+} signal of the spectra of figure 6. The results are shown in figure 7. Band C is mainly polarized along ***b*** while bands A and B both display the same polarization

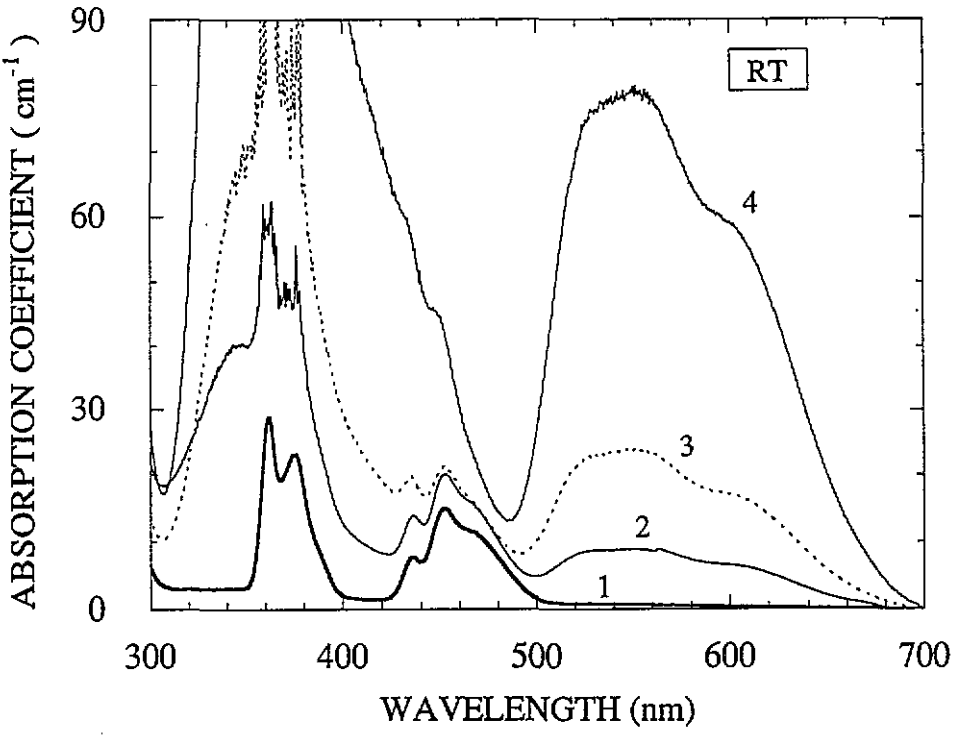

Figure 2. Optical absorption spectra of the pure and Cu^{2+} doped TMA_2MnBr_4 crystals at room temperature. Spectra 1, 2, 3 and 4 correspond to the pure (0 ppm), C1 (700 ppm), C2 (2000 ppm) and C3 (7400 ppm) crystals, respectively.

mainly along the ***a*** direction. Moreover, band A shows a complex structure which is formed by three components at about 603 (A1), 560 (A2) and 525 nm (A3). A shoulder at about 420 nm is clearly observed in these spectra. The corresponding band called C′ is mainly polarized along ***b*** and its bandshape has been enhanced in the inset of figure 7. This has been done by subtracting 0.6 times spectrum ***b*** from spectrum ***a*** in order to eliminate band B in the final spectrum. This procedure allows the position of the peak C′ to be determined precisely.

Following the method of [5], we have analysed the polarization character of these bands by means of the so called relative band intensities, defined as

$$I_{ri} = I_i / \sum_{j=a,b,c} I_j \qquad (1)$$

where I_i and I_j represent the integrated band intensities in the polarized spectrum along the i and j directions, respectively. The summation extends over the three orthogonal directions ***a***, ***b*** and ***c***.

The I_{ri} values derived from the spectra of figure 7 are given in table 1. The relative contributions as well as the peak positions of A1, A2 and A3 were calculated by fitting the whole A band to the sum of three gaussians. The fitting accuracy measured in terms of the chi square parameter was in all cases less than 10^{-4}.

The temperature dependence of the OA spectrum of sample C2 in the 10–300 K range is depicted in figure 8. In this study we focus on the variations undergone by the $^4T_1(G)$,

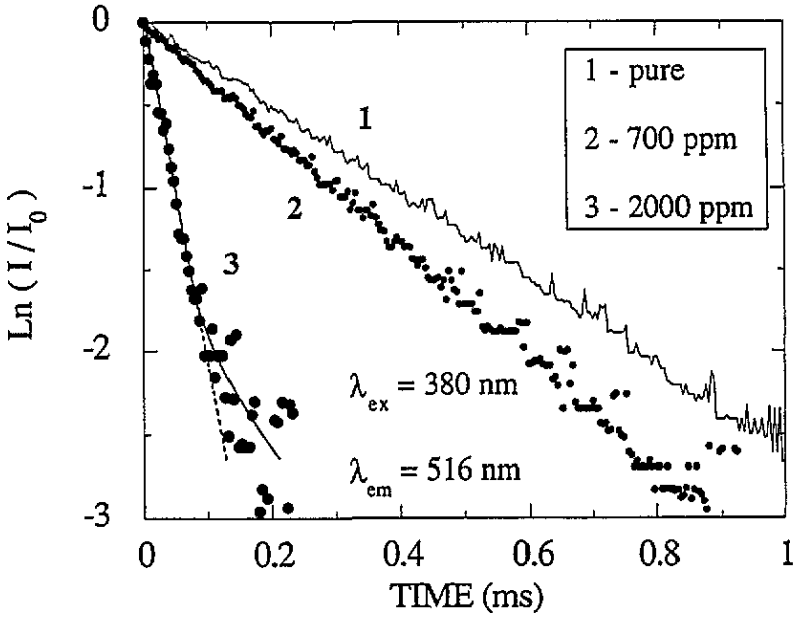

Figure 3. Luminescence decays for the $TMA_2MnBr_4:Cu^{2+}$ crystals at room temperature. Lifetime values of 385, 300 and 50 μs were obtained from the linear part of the $\ln(I/I_0)$ versus time plots 1, 2 and 3, respectively.

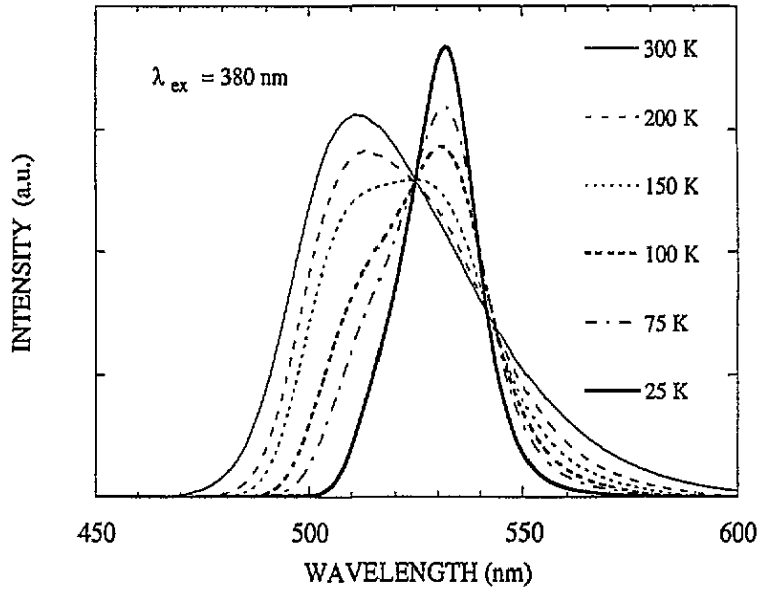

Figure 4. Temperature dependence of the luminescence spectrum of $TMA_2MnBr_4:Cu^{2+}$ sample C1 (700 ppm) in the 25–300 K range.

$^4T_2(G)$ and $^4A_1$, $^4E(G)$ bands of the $MnBr_4^{2-}$ and on the band A associated with the Cu^{2+}. The three components of band A, which are well resolved in the low temperature spectra,

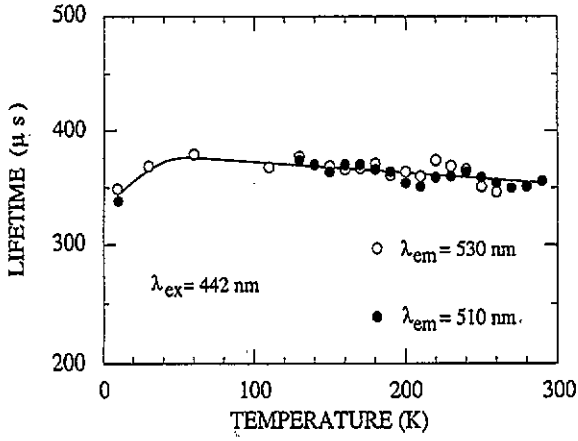

Figure 5. Lifetime temperature dependence of the $TMA_2MnBr_4:Cu^{2+}$ (sample C1—700 ppm) luminescence at 530 nm (○) and 510 nm (●). These wavelengths correspond to the luminescence band maxima observed at 10 and 300 K, respectively.

experience a redshift of 200 cm^{-1} from 10 to 300 K (figure 9) in contrast with the $^4T_1(G)$ and $^4T_2(G)$ bands of $MnBr_4^{2-}$ which shift about 200 cm^{-1} but to higher energies as a result of a decrease in the CF parameter $10Dq$ by thermal expansion effects. At $T = 10$ K, the Mn^{2+} bands display a rich vibronic structure in which progressions of the totally symmetric a_1 vibrations, $\hbar\omega = 163$ cm^{-1}, are dominant [16]. It is worth noting that the three components of band A, peaking at 595.2, 557.1 and 520.3 nm in the OA spectrum at $T = 10$ K, coincide with the *mystery bands* observed in the $T = 20$ K OA spectrum of the *nominally pure* TMA_2MnBr_4 [16].

Figure 10 shows the polarized OA spectrum of C3, the most highly doped $TMA_2MnBr_4:Cu^{2+}$ sample, in the NIR region (1000–2200 nm). The OA spectrum of the undoped crystal is also included for comparison. The high absorption of the crystal induced by the TMA group vibrations prevents any spectroscopic study of Cu^{2+} above 2200 nm.

A prominent broad band mainly polarized along the ***b*** direction is observed at about 1300 nm. This band is not detected in the pure TMA_2MnBr_4 and is, therefore, associated with the Cu^{2+} centres. On the other hand, the nearly isotropic peaks at 1170, 1360 and 1700 nm, also observed in the pure crystal, correspond to vibrational overtones of the TMA groups.

The ED oscillator strengths of all these bands have been calculated by using the equation [22]

$$f = 3.89 \times 10^{-8} \frac{n}{(n^2+2)^2} \int \epsilon \, dE \tag{2}$$

where ϵ is the molar extinction coefficient, E is the transition energy (cm^{-1}) and $n = 1.5$. The integral extends over the whole band including the three orthorhombic polarizations with a factor of $\frac{1}{2}$ for the x, y polarized bands.

Table 2 summarizes the experimental oscillator strengths, calculated using equation (2), as well as the peak position, polarization and assignment of absorption bands associated with the Cu^{2+} complexes. An analysis of these data is given in the next section.

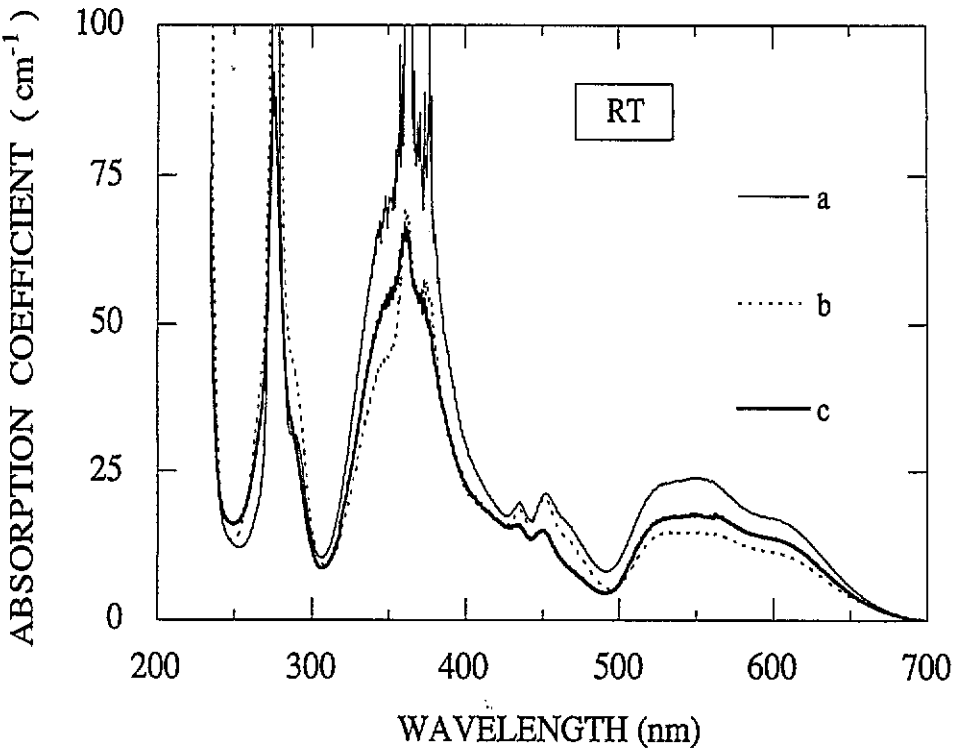

Figure 6. Polarized OA spectra of $TMA_2MnBr_4:Cu^{2+}$ (sample C2—2000 ppm) at room temperature. (001) and (010) single-crystal plates were used for obtaining the spectra with E parallel to the a, b and c orthorhombic directions. The zero absorption level was taken at 700 nm for the three spectra.

4. Analysis and discussion

4.1. Luminescence properties: influence of Cu^{2+} impurities

The presence of Cu^{2+} impurities in TMA_2MnBr_4 with an intense absorption band in the same spectral region as the Mn^{2+} emission profoundly influences its luminescence properties. Two processes are expected to be dominant: (1) Radiative $Mn^{2+} \rightarrow Cu^{2+}$ energy transfer in which photons emitted by Mn^{2+} are absorbed by Cu^{2+}. This mechanism would influence both the intensity and spectrum of the luminescence but would not affect the luminescence lifetime. (2) Non-radiative $Mn^{2+} \rightarrow Cu^{2+}$ energy transfer. This would induce changes in both the time dependence and the total intensity of the luminescence depending on the particular transfer rates.

The first of these processes is well reflected in the spectra of figures 1 and 4. The Cu^{2+} absorption band A at 555 nm acts as a filter which modifies the luminescence spectrum. Depending on the Cu^{2+} concentration the bandshape of the outward luminescence is deformed and its intensity is attenuated. An increase of the Cu^{2+} concentration shifts the luminescence band to higher energies because the crystal absorbance progressively increases from 490 to 550 nm. The sharp decrease of the luminescence intensity observed in figure 1 is explained by several processes: attenuation experienced by the luminescence through

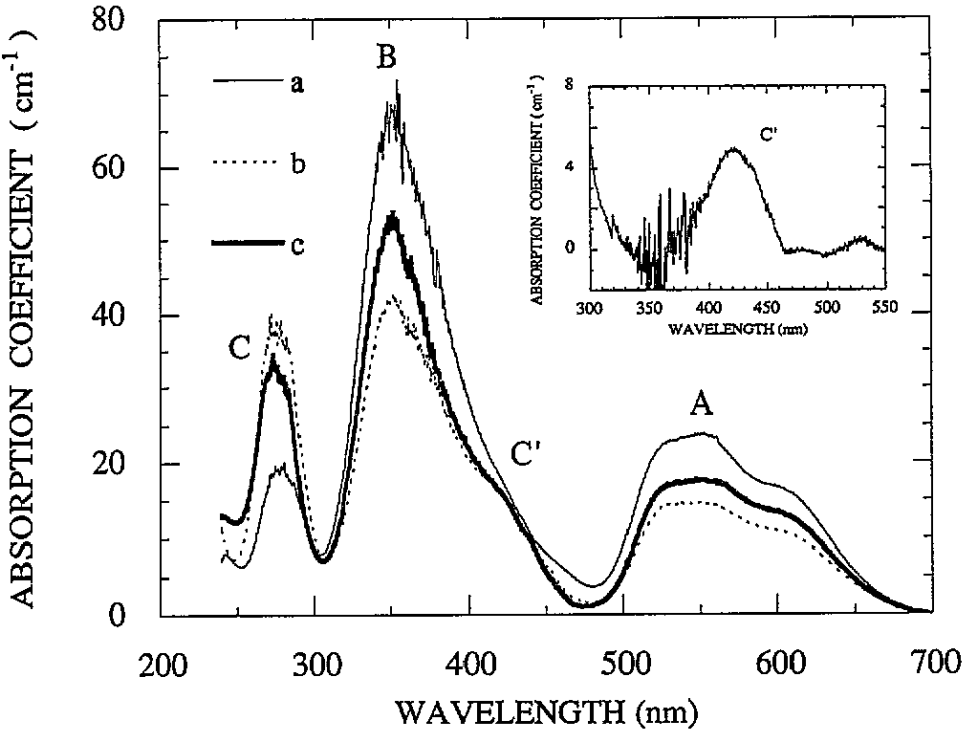

Figure 7. Polarized OA spectra of $TMA_2MnBr_4:Cu^{2+}$ (sample C2—2000 ppm) at room temperature after subtracting the Mn^{2+} contribution. The spectra were obtained by subtracting the OA spectra of the pure crystal (inset of figure 1) from those given in figure 6. The inset shows the OA spectrum corresponding to the *b*-polarized spectrum minus 0.6 times the *a*-polarized one. This is done in order to eliminate bands A and B and to enhance band C′ in the final spectrum.

Table 1. e_1, e_2 and e_3 denote the square components of the unitary vectors e_1, e_2 and e_3 pointing along the S_4 axes of the $MnBr_4^{2-}$ tetrahedra in TMA_2MnBr_4 with respect to the orthogonal *a*, *b* and *c* directions, respectively. I_{ii}, with $i = a, b$ and *c*, are the relative intensities of bands A, B and C, defined in equation (1). The last two columns show the polarization type of the bands: *x*, *y* type for bands A and B, and *z* type for C.

i direction	e_1	$e_2(e_3)$	I_{ii}^{A}	I_{ii}^{B}	I_{ii}^{C}	$I_{ii}^{C} + 2I_{ii}^{A}$	$I_{ii}^{C} + 2I_{ii}^{B}$
a	0	0.51	0.40	0.44	0.20	1.00	1.08
b	0.60	0.18	0.27	0.25	0.47	1.01	0.97
c	0.34	0.31	0.33	0.31	0.33	0.99	0.95

band A and by the excitation beam through band B; and the non-radiative $Mn^{2+} \rightarrow Cu^{2+}$ energy transfer proposed above.

The appearance of a new component in the low-temperature luminescence spectra (figure 4), also observed in other compounds containing $MnBr_4^{2-}$ complexes [23, 24], is not associated in our case either with non-equivalent $MnBr_4^{2-}$ units or with different excited states; instead, it corresponds to the same $^4T_1 \rightarrow {}^6A_1$ transition of Mn^{2+}. The presence of these two components is explained by taking into account the fact that the variation of band A with temperature (figure 8) modifies the crystal transmittance. The evolution of the

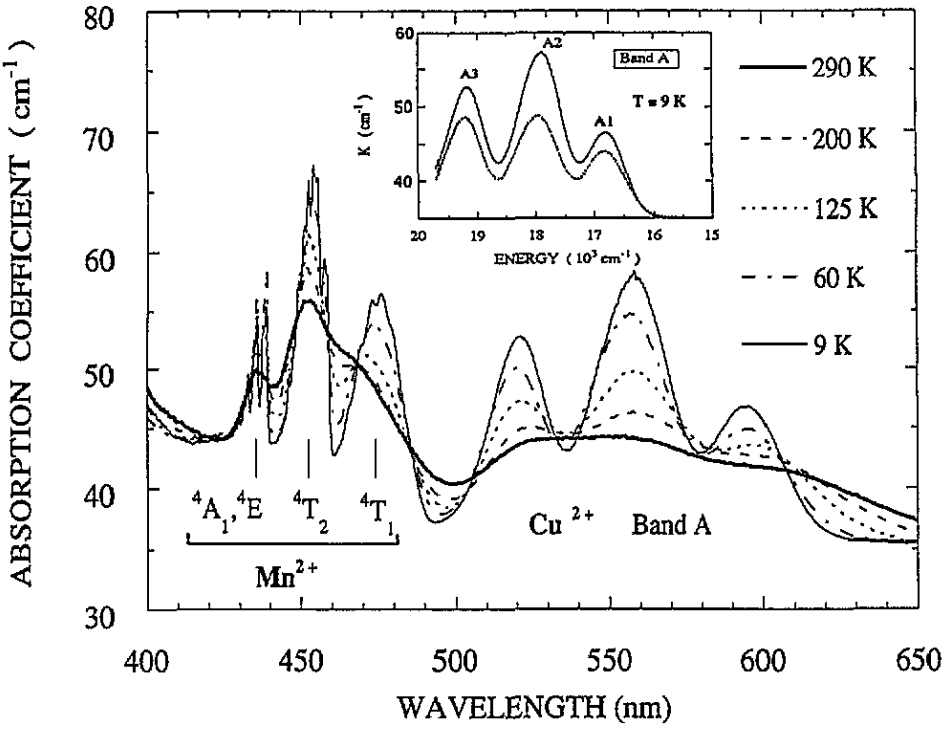

Figure 8. Temperature dependence of the polarized OA spectrum of $TMA_2MnBr_4:Cu^{2+}$ (sample C1—700 ppm) in the 400–650 nm range. The inset shows the $T = 9$ K polarized OA spectra of band A along the two extinction directions.

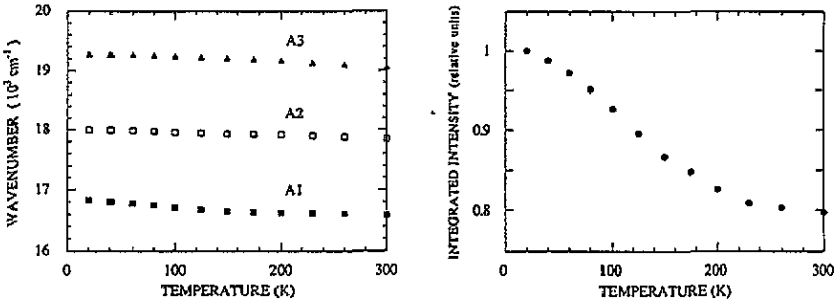

Figure 9. Variation of the peak positions of the three components (A1, A2 and A3) of band A as well as the total integrated intensity with the temperature. Peak positions were obtained by fitting band A to the sum of three Gaussians as is explained in the text.

luminescence spectrum observed in figure 4 is a direct consequence of the band narrowing of the A3 component at 520 nm together with the 300 cm^{-1} redshift experienced by the emission band from 300 to 10 K. The isosbestic point at 525 nm roughly corresponds to the maximum of the A3 absorption band and the luminescence bandshape at low temperature corresponds to the convolution of the real luminescence spectrum and the transmittance window between 520 and 560 nm.

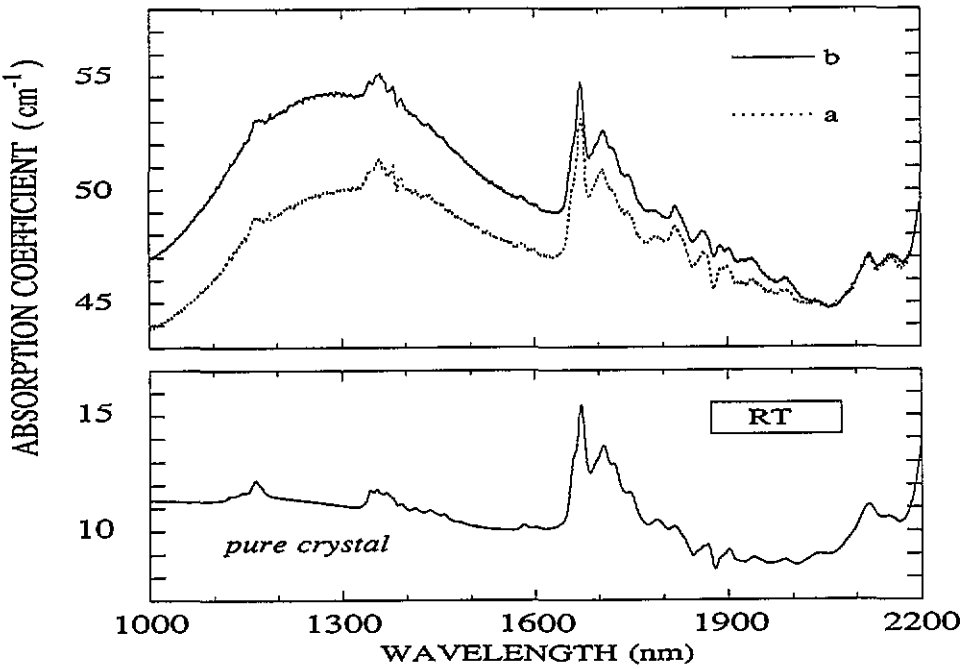

Figure 10. Polarized OA spectra of $TMA_2MnBr_4:Cu^{2+}$ (sample C3—7400 ppm) at room temperature in the 1000–2200 nm NIR range. A (001) single crystal was employed for obtaining the spectra with E parallel to the a and b orthorhombic directions. The OA spectra of the pure TMA_2MnBr_4 crystal is also included.

This interpretation is also supported by the fact that the lifetime and its temperature dependence are the same for the two components (figure 5), indicating that the emission bands at 530 and 510 nm correspond to the same electronic $^4T_1 \rightarrow {}^6A_1$ transition, as is expected for this crystal with equivalent $MnBr_4^{2-}$ complexes.

The results of figure 3 show that an increase in the Cu^{2+} concentration leads to a decrease of the luminescence lifetime, with a progressive deviation from the exponential behaviour in sample C2, as well as a pronounced drop in the total luminescence intensity similar to that observed in Cu^{2+} doped $TMAMnCl_3$ [1–3] and $TMAMnBr_3$ [4]. However, the microscopic origin of these phenomena is quite different. While in the latter systems it is associated with the existence of migration between exchange coupled Mn^{2+} and subsequent transfer to Cu^{2+}, the long distance between independent $MnBr_4^{2-}$ units (8 Å) in TMA_2MnBr_4 [25, 26] prevents migration among Mn^{2+} in this crystal. Nevertheless, Cu^{2+} doped TMA_2MnBr_4 crystals exhibit suitable conditions for either radiative or non-radiative direct energy transfer from Mn^{2+} to the non-luminescent Cu^{2+}. In fact, the high oscillator strength of the first CT band of the Cu^{2+} (0.018) and the large overlap between this band and the Mn^{2+} emission favour both types of transfer. The effect of the Cu^{2+} concentration on the intensity decay (figure 3) must be explained in terms of a direct non-radiative energy transfer mechanism. In particular, the dipole–dipole transfer rate between one Mn^{2+} and one Cu^{2+} ion can easily be calculated [27] using

$$\omega^{DD}_{Mn\rightarrow Cu} = (\tau^0_{Mn})^{-1}(R_0/R_{Mn-Cu})^6 \qquad (3)$$

where τ^0_{Mn} is the Mn^{2+} radiative lifetime, R_{Mn-Cu} is the Mn^{2+}–Cu^{2+} distance and R_0 is the

Table 2. Charge transfer (CT) band assignment of $CuBr_4^{2-}$ in $TMA_2MnBr_4:Cu^{2+}$. The corresponding data for $TMA_2MnCl_4:Cu^{2+}$ [5] are also included. The highest-energy $4a_1 \rightarrow 4b_2$ crystal field (CF) transition is also given. f is the experimental oscillator strength. Energies are in cm^{-1}.

				$TMA_2MnCl_4:Cu^{2+}$		$TMA_2MnBr_4:Cu^{2+}$		
	Transition	Type	Polarization	Peak Energy	f	Peak Energy		f
	$4a_1 \rightarrow 4b_2$	CF	z	8200	—	7700		~0.001
	$1a_2(\text{n.b.}) \rightarrow 4b_2$	CT		—	—		16 580(A1) 0.0061 17 845(A2) 0.0032 19 055(A3) 0.0084	
(A)	$4e \rightarrow 4b_2$	CT	x, y	24 300	0.022	18 000		0.018
(C′)	$3a_1 \rightarrow 4b_2$	CT	z	~29 500	<0.001	23 800		~0.01
	$3e \rightarrow 4b_2$	CT	x, y	—	—	—		—
(B)	$2e \rightarrow 4b_2$	CT	x, y	33 700	0.073	28 400		0.06
(C)	$2a_1 \rightarrow 4b_2$	CT	z	41 000	0.049	36 100		~0.05

critical interaction distance, defined in the following equation, for which the $Mn^{2+} \rightarrow Cu^{2+}$ transfer rate is $(\tau^0_{Mn})^{-1}$:

$$R_0 = \left(\frac{3 f_{Cu} e^2 \phi_{Mn} \Omega}{4(2\pi n \tilde{\nu}_{da})^4 mc^2} \right)^{1/6} \tag{4}$$

where f_{Cu} is the oscillator strength of the CT band, and

$$\Omega = \int g_{Cu}(\tilde{\nu}) G_{Mn}(\tilde{\nu}) \, d\tilde{\nu} \qquad (\tilde{\nu} = \text{wavenumber}).$$

$G_{Mn}(\tilde{\nu})$ and $g_{Cu}(\tilde{\nu})$ are the normalized bandshapes of the emission and CT bands, respectively. Other parameters defined in equation (4) have the usual meaning [27].

Taking for the present case $f_{Cu} = 0.018$, $\phi_{Mn} = 1$, $\Omega = 0.1647$ ($1/10^3$ cm^{-1}), $\tilde{\nu} = 19.5$ (10^3 cm^{-1}) and $n = 1.5$, we obtain $R_0 = 30$ Å.

In the present systems, the average Cu^{2+}–Cu^{2+} distances are 54, 38 and 25 Å for the C1, C2 and C3 crystals. This means that the number of Mn^{2+} ions within the critical interaction sphere varies from 15% in C1, to 50% and 100% in C2 and C3, respectively. These values allow us to explain qualitatively the experimental results of figure 3. Faster non-exponential decays are observed in C2, where half of the Mn^{2+} are inside the critical sphere. The dramatic decrease of the luminescence intensity in C3 (figure 1) reveals the high $Mn^{2+} \rightarrow Cu^{2+}$ transfer rate, which is estimated to be 7.8×10^4 s^{-1} for the largest Mn^{2+}–Cu^{2+} distance. This mechanism explains the extremely low luminescence of sample C3, whose efficiency should decrease by about one order of magnitude. Further investigation along these lines using pulsed light in order to obtain precise decays $I(t)$ will be done in the near future.

It is worth pointing out that the reason why these phenomena have not been observed in $TMA_2MnCl_4:Cu^{2+}$ is that the first CT band of the $CuCl_4^{2-}$ complexes, located at 412 nm, is far from the Mn^{2+} luminescence band, which peaks at 522 nm at 300 K [28, 29].

4.2. Polarization analysis of the $CuBr_4^{2-}$ optical absorption spectrum

The oscillator strengths and the transition energies of the absorption bands A, B and C of the spectra of figure 7 clearly indicate that these bands correspond to CT transitions of Cu^{2+} having Br^- ligands. Furthermore, the similarity between these CT spectra and the corresponding ones for $TMA_2MnCl_4:Cu^{2+}$, associated with $CuCl_4^{2-}$ D_{2d} symmetry complexes [5], strongly suggests that distorted $CuBr_4^{2-}$ complexes with D_{2d} symmetry are responsible for the spectra of figure 7. This view is also supported by the OA spectra of solutions of TMA_2CuBr_4 containing $CuBr_4^{2-}$ units [30–32]. In addition, the CT bands A, B, C and C′ in $TMA_2MnBr_4:Cu^{2+}$ display the same polarization with respect to the $\boldsymbol{a}$, $\boldsymbol{b}$ and $\boldsymbol{c}$ directions as the corresponding ones in $TMA_2MnCl_4:Cu^{2+}$. The major difference is that the overall spectrum for the bromide is shifted by about 5000 cm^{-1} to lower energies (table 2). This energy difference is a direct consequence of the smaller optical electronegativity of the Br^- ligand, $\chi = 2.8$, compared to that of the Cl^-, $\chi = 3.0$, and agrees reasonably well with the value expected on the basis of Jørgensen's empirical rule [33]: $\Delta E \cong 30\,000 \Delta\chi = 6000$ cm^{-1}.

Moreover, the polarization analysis performed on these spectra supports a D_{2d} symmetry distortion of the Cu^{2+} substituted $MnBr_4^{2-}$. A local D_{2d} symmetry is usually found in tetracoordinated complexes when a strong Jahn–Teller (JT) ion like Cu^{2+} is involved [34]. Such a D_{2d} distortion in T_d complexes corresponds to flattened tetrahedra in accordance

with the fact that vibrational modes of e (bending) symmetry in T_d are the most relevant in JT coupling [35]. This distortion would take place along one of the three improper S_4 axes of the undistorted tetrahedron and consequently the CT symmetry allowed electric dipole transitions would be polarized either along z or in the perpendicular x–y plane, with z being directed along the S_4 axis around which the distortion takes place.

The analysis of the relative intensities of the bands A, B and C (table 1), using the procedure followed in [5], clearly demonstrates that A and B are x, y polarized while C is z polarized. Moreover, the relative intensity values allow us to determine the $CuBr_4^{2-}$ orientation within the lattice. The x-ray structural data for TMA_2MnBr_4 [25] show that the four $MnBr_4^{2-}$ tetrahedra in the orthorhombic unit cell are located in (4c) (figure 11). The square components of the e_1, e_2 and e_3 unitary vectors along the three S_4 axes are the same for all the tetrahedra. By inspecting table 1, it is concluded that the $CuBr_4^{2-}$ distortion takes place around the e_1S_4 axis lying in (100) planes. This result resembles the experimental observations in the pure TMA_2CuBr_4 where $CuBr_4^{2-}$ units are distorted along e_1. As in the case of TMA_2MnCl_4:Cu^{2+}, the data of table 1 indicate that the $CuBr_4^{2-}$ distortion axis has a net component outside the (100) plane. The experimental values of I_{ri} can be reproduced well if we take into account the fact that the $CuBr_4^{2-}$ complexes formed are rotated 30° either clockwise or counterclockwise around the c direction. This means that TMA_2MnBr_4 should also exhibit an orientational disorder in the orthorhombic phase associated with $CuBr_4^{2-}$ rotations around the c-axis similar to that observed in TMA_2MnCl_4:Cu^{2+} crystals [6]. Evidence of this disorder has been obtained for the family of crystals TMA_2MBr_4 (M = Zn, Cu, Mn) using x-ray diffraction techniques [25, 26, 36–39].

Since no abrupt changes are observed either in the relative CT intensities or in the peak positions when temperature is varied, we conclude that no phase transition involving reorientational motions of the $CuBr_4^{2-}$ tetrahedra takes place in the range 10–270 K. This result is in agreement with the experimental observations of Gesi [40] using dielectric measurement: he did not find any evidence of phase transitions in this crystal at 1 atm between 77 and 276 K. However, it is rather different from findings in TMA_2MnCl_4:Cu^{2+} crystals where small jumps of the band intensities were observed at the phase transition temperatures [6].

4.3. Charge transfer and crystal field band assignment

Within a molecular orbital (MO) framework, there are five possible ED allowed CT transitions in $CuBr_4^{2-}$ complexes of D_{2d} symmetry (figure 12). These transitions involve electronic jumps from mainly Br^- MOs of e and a_1 symmetry to the unpaired mainly Cu^{2+} ($d_{x^2-y^2}$) MO of b_2 symmetry. The $e \rightarrow b_2$ is x, y polarized while the $a_1 \rightarrow b_2$ is z polarized.

The CT band assignment given in table 2 was made on the basis of both their polarization and the π or σ character of the ligand MOs involved in the transition, following the same scheme employed in the assignment made for $CuCl_4^{2-}$ [5, 41]. Transitions coming from σ orbitals are expected to have higher oscillator strengths due to the larger overlaps with the 3d wavefunctions of Cu^{2+}. Bands B and C, at 28 400 and 36 100 cm^{-1}, were assigned to transitions from the mainly Br^- (p_σ) 2e and $2a_1$ MOs to the $4b_2$ MO, respectively, given that their oscillator strengths, 0.06 and 0.05, are much higher than those corresponding to the bands C′ and A, ~ 0.01 and 0.018, respectively. In the case of $CuCl_4^{2-}$ complexes, where the mainly Cl^- (p_π) 3e and $3a_1$ appear close together in the energy level diagram [5], the lowest intensity band C′ was associated with either the $3e \rightarrow 4b_2$ (Cs_2CuCl_4) or the $3a_1 \rightarrow 4b_2$ (TMA_2MnCl_4:Cu^{2+}) transitions depending on whether their respective polarizations were (x, y) or z. In TMA_2MnBr_4:Cu^{2+}, this band at 23 800 cm^{-1} is assigned to $3a_1 \rightarrow 4b_2$ in accordance with its mainly z polarization. This assignment agrees with

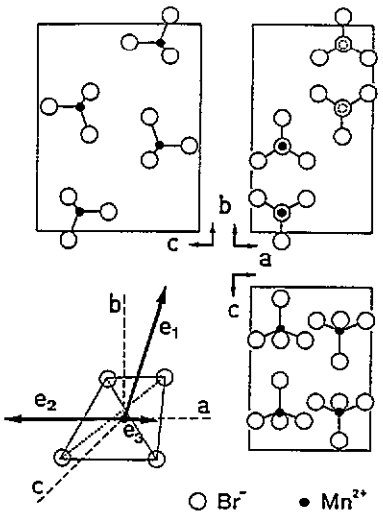

Figure 11. (100), (010) and (001) projections of the TMA_2MnBr_4 unit cell (*Pmcn* space group). Only the four $MnBr_4^{2-}$ units at (4c) sites were drawn. The figure on the left side at the bottom shows the unitary vectors e_1, e_2 and e_3 along the S_4 axes of the $MnBr_4^{2-}$ tetrahedron. $CuBr_4^{2-}$ distortions of D_{2d} symmetry would correspond to a flattened tetrahedron along one of the S_4 axes. The trans-Br–Cu–Bar angle, θ, equal to 109° for regular tetrahedra, defines the degree of distortion of these $CuBr_4^{2-}$ complexes.

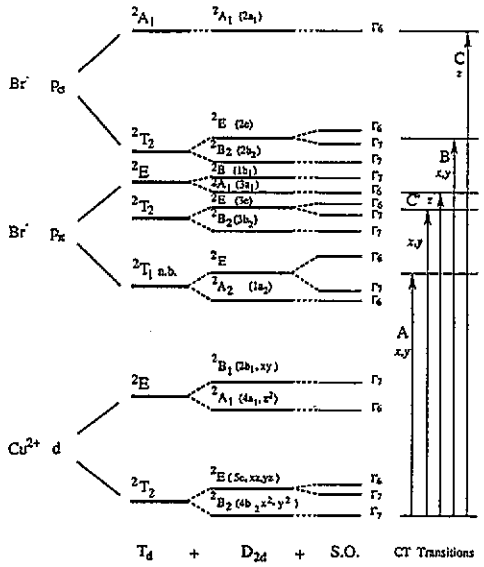

Figure 12. Proposed energy level diagram of the $CuBr_4^{2-}$ electronic states in T_d symmetry under the influence of the D_{2d} distortion field and spin–orbit interaction. The unpaired one-electron level of each state is given in parenthesis following the same notation as used for $CuCl_4^{2-}$ in [5]. The CT states are scaled according to the energies and polarizations observed in the OA spectrum. The arrows indicate the symmetry allowed electric dipole transitions.

that given for $CuBr_4^{2-}$ in solutions of TMA_2CuBr_4, where the singlet character of the ligand MO associated to the C′ band was demonstrated by MCD measurements [31].

The first x, y-polarized CT band, at 555 nm, shows a triplet structure whose components are well resolved in the 10 K OA spectrum. Though a similar structure has already been found by Bird and Day [30] in TMA_2CuBr_4 solutions at 77 K, it is not observed in Cs_2CuCl_4 where only one band at 403 nm ($4e \rightarrow 4b_2$) and a small shoulder ($1a_2 \rightarrow 4b_2$) at about 435 nm were detected [42–44]. Bird and Day assigned the three components of $CuBr_4^{2-}$ CT band A to transitions from the ground state to the non-bonding $^2T_1$ CT state within the tetrahedral symmetry which is split by both the D_{2d} static distortion and the large Br^- spin–orbit interaction ($\xi_{4p} = 2480\ cm^{-1}$) in $^2E(\Gamma_6+\Gamma_7)+{}^2A_2(\Gamma_6)$ (double group D_{2d} irrep). The mixing between the $\Gamma_6(^2A_2)$ and the $\Gamma_6(^2E)$ states, induced by the spin–orbit interaction of the Br^- ligands, gives ED oscillator strength to the $^2B_2 \rightarrow {}^2A_2$ transition which would be forbidden on the basis of only D_{2d} distortions.

In the present case, the bands A1, A2 and A3 are analogously assigned to $^2A_2(\Gamma_6)$ and $^2E(\Gamma_6 + \Gamma_7)$, respectively. However, the intensity of band A1 and the splitting between A2 and A3 are different in the two systems. In particular, the A2–A3 splitting increases from 850 cm^{-1} in TMA_2CuBr_4 [30] to 1300 cm^{-1} in $TMA_2MnBr_4:Cu^{2+}$, and the ratio of the intensity of A1 to the total intensity of band A is twice as high for the latter case. However, it is noteworthy that the mean position of band A taken as the arithmetic average of the transition energies of A1, A2 and A3 has the same value, 18 000 cm^{-1}, in both systems.

The different $^2T_1$ splitting pattern found in these systems gives direct evidence of the different contributions of the spin–orbit interaction and the tetragonal crystal field in the two $CuBr_4^{2-}$ complexes. We have calculated this splitting in a first-order approximation by diagonalizing the effective Hamiltonian

$$H = -\lambda L \cdot S + H_{CF} \tag{5}$$

where λ is the spin–orbit coupling constant within the sixfold $^2T_1$ state, L is the effective angular momentum operator and H_{CF} is the tetragonal component of the crystal field. Figure 13 shows the results of these calculations. The $^2T_1$ splitting is given in units of λ as a function of the parameter $\beta = \Delta/\lambda$. The energy difference between the ^2E and $^2A_2$ states induced by the tetragonal crystal field is represented by Δ. Note that in the limit $\Delta \gg 1$, the energy difference between the two highest states Γ_6 and Γ_7 tends to λ, which corresponds to the spin–orbit splitting within ^2E.

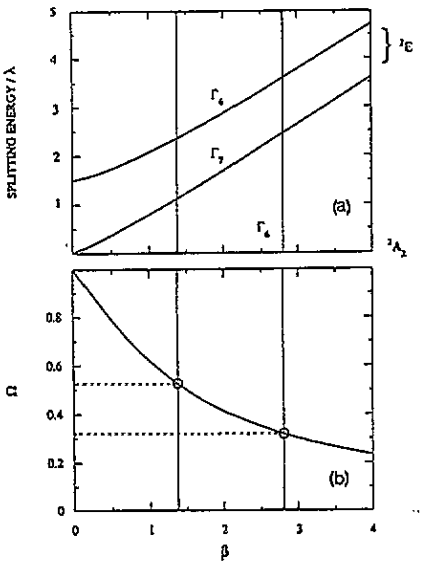

Figure 13. (*a*) Splitting of the $^2T_1$ NB (T_d) CT state as a function of $\beta = \Delta/\lambda$. Δ and λ are the tetragonal splitting between ^2E and $^2A_2$ states and the spin–orbit coupling constant, respectively. The energies are given with respect to the $\Gamma_6(^2A_2)$ state in units of λ. (*b*) variation of the parameter $\Omega = [E(\Gamma_6(^2E)) - E(\Gamma_7(^2E))]/[E(\Gamma_6(^2E)) - E(\Gamma_6(^2A_2))]$ with β. Values of $\beta = 2.80$ and 1.38 have been determined through this curve from the experimental values of $\Omega = 0.32$ and 0.52 in TMA_2CuBr_4 [30] and $TMA_2MnBr_4{:}Cu^{2+}$, respectively.

Taking λ and Δ as fitting parameters, the triplet structure observed in $CuBr_4^{2-}$ is well reproduced for $\lambda = 1030$ and 750 cm^{-1}, and $\Delta = 1420$ and 2100 cm^{-1} in $TMA_2MnBr_4{:}Cu^{2+}$ and TMA_2CuBr_4, respectively.

Two results should be underlined. (1) The spin–orbit coupling constant is much lower than the expected value, $\lambda = 1/2\xi_{4p} = 1240$ cm^{-1}, in the former compound [30], which is in turn responsible for the weak splitting (850 cm^{-1}) displayed by the ^2E state. (2) The D_{2d} distortion in $TMA_2MnBr_4{:}Cu^{2+}$, measured through the parameter Δ, is smaller than in TMA_2CuBr_4. Both of these facts favour an increase of the ED oscillator strength of the $^2B_2(\Gamma_6) \rightarrow {}^2A_2(\Gamma_6)$ transition in $TMA_2MnBr_4{:}Cu^{2+}$, which explains the relatively high oscillator strength of its A1 band. Furthermore, this analysis explains why the highest Γ_6 state lies above the Γ_7 state. The polarization measurements of figure 8 also support this view. In fact, though bands A1, A2 and A3 display nearly the same x, y polarization, a simple inspection of the OA spectra at 10 K shows that while A1 and A3 have exactly the same intensity ratios in both polarizations, this ratio is slightly different in A2.

Concerning the CF spectrum (figure 10), the z-polarized broad band at 7700 cm^{-1} is assigned to the transition from the $4a_1(3z^2 - r^2)$ to the $4b_2$ mainly Cu^{2+} MOs. Other CF bands at lower energies are masked in the spectrum by the overtones of the TMA groups at 6000 cm^{-1}. Thus, the CF spectrum of $TMA_2ZnBr_4:Cu^{2+}$ and its assignment reported by De [45] must be taken with caution. In fact, the three absorption bands at 1100, 1350 and 1670 nm assigned by this author to $CuBr_4^{2-}$ CF bands coincide exactly with the TMA group overtones that we observe in the OA spectrum of the pure TMA_2MnBr_4 (figure 10).

Finally, it is worth noting the red shift of 500 cm^{-1} experienced by the $4a_1 \rightarrow 4b_2$ CF transition when passing from $TMA_2MnCl_4:Cu^{2+}$ to $TMA_2MnBr_4:Cu^{2+}$. This shift, which is also observed in pure compounds where this band changes from 9000 cm^{-1} in Cs_2CuCl_4 [42] and TMA_2CuCl_4 [46], to 8000 and 8300 cm^{-1} in Cs_2CuBr_4 [47] and TBA_2CuBr_4 [48], respectively, reflects the weaker ligand field strength of the Br^- ligands. However, such red shifts can also be induced by reducing the D_{2d} distortion through a decrease of the trans-X–Cu–X bond angle θ of the CuX_4^{2-} complex. This effect, which is experimentally well known for $CuCl_4^{2-}$ [11–16], has not yet been evidenced for $CuBr_4^{2-}$ in view of the small number of title compounds.

Accordingly, the variation in the CF band observed in $CuBr_4^{2-}$ when passing from Cs_2CuBr_4 (8000 cm^{-1}) or TBA_2CuBr_4 (8300 cm^{-1}) to $TMA_2MnBr_4:Cu^{2+}$ (7700 cm^{-1}) can be explained in these terms. This variation is very similar to that found in TMA_2CuCl_4 (9000 cm^{-1}) and $TMA_2MnCl_4:Cu^{2+}$ (8200 cm^{-1}) which is associated with a reduction of the distortion angle θ from 129° to 124° [5, 49, 50]. The red shift of the CF band as well as the reduction of the $^2T_1$ CT state splitting, Δ, are then interpreted in terms of weaker D_{2d} distortion of the $CuBr_4^{2-}$ tetrahedra of the doped crystals considered here.

Acknowledgment

This work has been supported by the CICYT under project no MAT 90-0668.

References

[1] Yamamoto H, McClure D S, Marzzacco C and Waldman M 1977 *Chem. Phys.* **22** 79
[2] Auerbach R A and McPherson G L 1986 *Phys. Rev.* B **33** 6815
[3] Knochenmuss R and Güdel H U 1987 *J. Chem. Phys.* **86** 1104
[4] Rodríguez W J, Auerbach R A and McPherson G L 1986 *J. Chem. Phys.* **85** 6442
[5] Marco de Lucas M C, Rodríguez F and Aramburu J A 1991 *J. Phys.: Condens. Matter* **3** 8945
[6] Marco de Lucas M C and Rodríguez F 1992 *Ferroelectrics* **125** 159
[7] Willet R D, Ferraro J R and Choca M 1974 *Inorg. Chem.* **13** 2919
[8] Harlow R L, Wells W J, Watt G W and Simonsen S H 1974 *Inorg. Chem.* **13** 2106
[9] Bray K L and Drickramer H G 1990 *J. Phys. Chem.* **94** 2159
[10] Scott B and Willet R D 1991 *J. Am. Chem. Soc.* **113** 5223
[11] Smith D W 1976 *Coord. Chem. Rev.* **21** 93
[12] Battaglia L P, Bonamartini Corradi A, Marcotrigiano G, Menabue L and Pellacani G C 1979 *Inorg. Chem.* **18** 148
[13] Bond M R, Johnson T J and Willet R D 1988 *Can. J. Phys.* **66** 963
[14] Harlow R L, Wells W J, Watt G W and Simonsen S H 1974 *Inorg. Chem.* **13** 2106
[15] Halvorson K E, Patterson C and Willet R D 1990 *Acta Crystallogr.* B **46** 508
[16] Vala M T, Ballhausen C J, Dingle R and Holt S L 1972 *Mol. Phys.* **23** 217
[17] Marco de Lucas M C and Rodríguez F 1990 *Rev. Sci. Instrum.* **61** 23
[18] Nikolic K, Canny B, Curie D, Gendrom F and Porte C 1985 *Fizika* **1** 27
[19] Wrighton M and Ginley D 1974 *Chem. Phys.* **4** 295
[20] Presser N, Ratner M A and Sundheim B R 1978 *Chem. Phys.* **31** 281

[21] Sundheim B R, Levy E and Howard B 1971 *J. Chem. Phys.* **57** 4492
[22] Griffith J S 1980 *The Theory of Transition-Metal Ions* (Cambridge: Cambridge University Press) p 57
[23] Lanver U and Lehmann G 1978 *J. Lumin.* **17** 225
[24] Marco de Lucas M C, Rodríguez F and Moreno M 1992 *Phys. Status Solidi* b **172** 719
[25] Hasebe K and Asahi T 1989 *Acta Cryst.* C **45** 841
[26] Hasebe K, Asahi T and Gesi K 1990 *Acta Crystallogr.* C **46** 759
[27] Blasse G 1984 *Energy Transfer Processes in Condensed Matter* (New York: Plenum)
[28] Marco de Lucas M C and Rodríguez F 1989 *J. Phys.: Condens. Matter* **1** 4251
[29] Marco de Lucas M C, Rodríguez F and Moreno F 1990 *Ferroelectrics* **109** 21
[30] Bird B D and Day P 1968 *J. Chem. Phys.* **49** 392
[31] Rivoal J C and Briat B 1974 *Mol. Phys.* **27** 1081
[32] Stein P, Jensen P W and Spiro T G 1981 *Chem. Phys. Lett.* **80** 451
[33] Jørgensen C K 1970 *Prog. Inorg. Chem.* **12** 101
[34] Puget R, Jannin M, Perret R, Godefroy L and Godefroy G 1990 *Ferroelectrics* **107** 229
[35] Sturge M D 1967 *Solid State Physics* vol 20 (New York: Academic) p 91
[36] Trouelan P, Lefebvre J and Derrollez P 1984 *Acta Crystallogr.* C **40** 386
[37] Hasebe K, Mashiyama H and Tanisaki S 1985 *Japan. J. Appl. Phys.* **24** 758
[38] Asahi T, Hasebe K and Gesi K 1988 *J. Phys. Soc. Japan* **57** 4219
[39] Madariaga G, Zúñiga F J, Paciorek W A and Bocanegra E H 1990 *Acta Crystallogr.* B **46** 620
[40] Gesi K 1983 *J. Phys. Soc. Japan* **52** 2931
[41] Bencini A and Gatteschi D 1983 *J. Am. Chem. Soc.* **105** 5535
[42] Ferguson J 1964 *J. Chem. Phys.* **40** 3406
[43] Sharnoff M and Reimann C W 1967 *J. Chem. Phys.* **46** 2634
[44] Desjardins S R, Penfield K W, Cohen S L, Musselman R L and Solomon E I 1983 *J. Am. Chem. Soc.* **105** 4591
[45] De D K 1983 *J. Chem. Phys.* **79** 535
[46] Willet R D, Liles O L and Michelson C 1968 *Inorg. Chem.* **6** 1885
[47] Karipides A G and Piper T S 1962 *Inorg. Chem.* **1** 970
[48] Ludwig W and Textor M 1971 *Helv. Chim. Acta* **54** 1143
[49] McGinnety J A 1972 *J. Am. Chem. Soc.* **94** 8406
[50] Clay R, Murray-Rust J and Murray-Rust P 1975 *Acta Crystallogr.* B **31** 289